3.4-THz quantum cascade laser based on longitudinal-optical-phonon scattering for depopulation

Cite as: Appl. Phys. Lett. **82**, 1015 (2003); https://doi.org/10.1063/1.1554479
Submitted: 02 December 2002 • Accepted: 27 December 2002 • Published Online: 10 February 2003

Benjamin S. Williams, Hans Callebaut, Sushil Kumar, et al.

3.4-THz quantum cascade laser based on longitudinal-optical-phonon scattering for depopulation

Benjamin S. Williams, Hans Callebaut, Sushil Kumar, and Qing Hu[a)]
Department of Electrical Engineering and Computer Science and Research Laboratory of Electronics, Massachusetts Institute of Technology, Cambridge, Massachusetts 02139

John L. Reno
Sandia National Laboratories, Department 1123, MS 0601, Albuquerque, New Mexico 87185-0601

(Received 2 December 2002; accepted 27 December 2002)

We report the development of a quantum cascade laser, at $\lambda = 87.2\ \mu$m, corresponding to 3.44 THz or 14.2 meV photon energy. The GaAs/$Al_{0.15}Ga_{0.85}As$ laser structure utilizes longitudinal-optical (LO) phonon scattering for electron depopulation. Laser action is obtained in pulsed mode at temperatures up to 65 K, and at 50% duty cycle up to 29 K. Operating at 5 K in pulsed mode, the threshold current density is 840 A/cm^2, and the peak power is approximately 2.5 mW. Based on the relatively high operating temperatures and duty cycles, we propose that direct LO-phonon-based depopulation is a robust method for achieving quantum cascade lasers at long-wavelength THz frequencies. © *2003 American Institute of Physics.*
[DOI: 10.1063/1.1554479]

The terahertz frequency range (1–10 THz) has long remained undeveloped, due mainly to the lack of compact, coherent radiation sources. Transitions between subbands in semiconductor heterostructure quantum wells were suggested as a method of generating radiation at customizable frequencies, including the terahertz, and indeed the first experimental observation of such radiation occurred at these long wavelengths.[1] However, the first laser based on an intersubband transition, the quantum cascade laser[2] was developed in the mid-infrared, and has been remarkably successful in covering that frequency range. Until very recently, no intersubband laser with an energy smaller than the longitudinal-optical (LO)-phonon energy ($E_{LO} \simeq 36$ meV in GaAs) had been made. Aside from the problem of long-wavelength-mode confinement, the major challenge is the difficulty of obtaining a population inversion between two subbands closely spaced in energy, while still maintaining sufficient oscillator strength for significant gain. The first terahertz quantum cascade lasers[3,4] were designed around chirped superlattice structures, which are characterized by large dipole strengths and fast electron removal from the lower state into a miniband of states. This removal occurs primarily through resonant tunneling and electron–electron scattering, as the miniband width is less than E_{LO}, and LO-phonons are involved only in cooling the electron distribution.

The direct use of LO-phonons for depopulation of the lower state offers two distinctive advantages. First, when a collector state is separated from the lower state by at least E_{LO}, depopulation can be extremely fast, and it does not depend much on temperature or the electron distribution. Second, the large energy separation provides intrinsic protection against thermal backfilling of the lower radiative state. Both properties are important in allowing higher temperature operation of lasers at longer wavelengths.

While fast scattering out of the lower radiative state is necessary, a long upper-state lifetime is also desirable. Early designs[5] addressed this problem by making the optical transition diagonal (i.e., between states in adjacent wells), so as to reduce upper-state overlap with the collector state. However, this resulted in a small oscillator strength, and in a broad emission linewidth due to interface roughness. A second design featured a vertical transition,[6] which improved the radiative overlap and had a relatively narrow linewidth (~2 meV), but depopulation was nonselective and slow, due to the thick barrier needed to reduce parasitic scattering from the upper state.

The present design combines the advantages of the two previous ones. The radiative transition is vertical, while the depopulation is highly selective, as only the lower state is anticrossed with a state in the adjacent well, where fast LO-phonon scattering takes place. As shown in Fig. 1(a), the four-quantum-well module grown in GaAs/$Al_{0.15}Ga_{0.85}As$ is based around a vertical transition between levels $n=5$ and $n=4$ (highlighted with thicker lines). At design bias (~64 mV/module), levels $n=4$ and $n=3$ are brought into resonance with an anticrossing gap of 5.3 meV,[7,8] enabling fast depopulation via LO-phonon scattering into the levels $n=2$ and $n=1$ ($\tau_{4\rightarrow(2,1)}=0.55$ ps). This allows the barrier to be kept relatively thick (38 Å), which limits parasitic scattering out of the upper state ($\tau_{5\rightarrow(2,1)}=7.1$ ps). These LO-phonon scattering rates are calculated using bulk GaAs phonon modes, which is a good approximation in structures with low Al content.[9] Assuming a fully coherent tunneling process between levels $n=3$ and 4,[10] additional depopulation of $n=4$ can take place via electron–electron scattering into $n=3$, which also has a short lifetime of $\tau_{3\rightarrow(2,1)}=0.46$ ps. Electrons collect in the anticrossed 2-1 doublet ($E_{21}=6.6$ meV) where they are injected into the $n=5$ state in the next module. In addition to parasitic scattering, the lifetime of the

a)Electronic mail: qhu@mit.edu

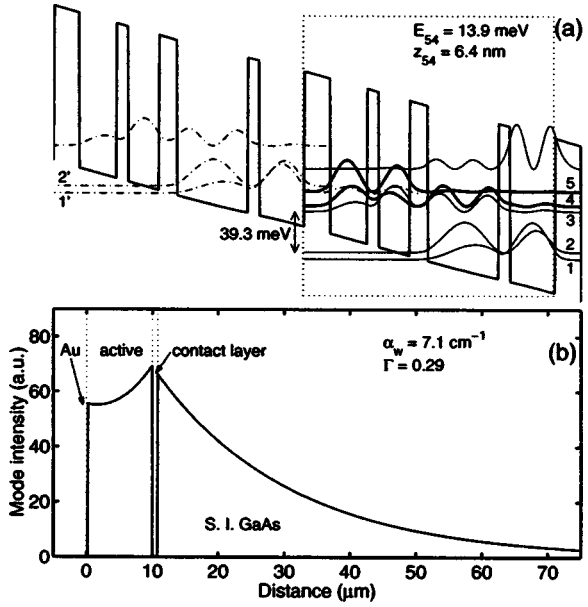

FIG. 1. (a) Conduction band profile calculated using a self-consistent Schrödinger and Poisson solver (80% band offset) biased at 64 mV/module, which corresponds to a field of 12.2 kV/cm. The four-well module is outlined. Beginning with the left injection barrier, the layer thickness in Å are 54/78/24/64/38/148/24/94. The 148-Å well is doped at $n=1.9\times10^{16}$ cm^{-3}, yielding a sheet density of 2.8×10^{10} cm^{-2}. (b) Optical mode profile of plasmon waveguide.

upper state is also determined by scattering from $5\rightarrow(4,3)$. At low temperatures, electron relaxation from $n=5$ into $n=4$ (and $n=3$) is suppressed as emission of LO-phonons is energetically forbidden, since the photon energy $E_{54}=13.9$ meV$<E_{\mathrm{LO}}$, and electron–electron scattering is expected to be the limiting lifetime mechanism.[11]

Molecular beam epitaxy was used to grow 175 cascaded modules, sandwiched between a 60-nm upper contact layer (doped to $n=5\times10^{18}$ cm^{-3}) and a bottom 800-nm contact layer ($n=3\times10^{18}$ cm^{-3}) on a semi-insulating GaAs substrate. Special care was taken to limit the drift in the growth rate to less than 0.7% over the entire growth, to ensure the accuracy of the doping concentration in the active region within 10%, and the Al fraction within 14.5%–15.5%. A top nonalloyed ohmic contact was made by evaporating Ti/Au layers on low-temperature-grown GaAs. Wet etching was used to define a 150-μm-wide ridge, and Ni/Ge/Au alloyed contacts were made to the lower contact layer at the bottom of the ridge. As the plasma frequency for this lower contact lies above the frequency of interest, a waveguide is formed between the upper metallic contact and the surface plasmons associated with the quasimetallic lower layer,[3,4,12] as seen in Fig. 1(b). A Fabry–Perot cavity was formed by cleaving the structure into a 1.18-mm-long bar, and the back facet was coated by evaporating Ti/Au over silicon nitride. The device was then mounted ridge side up on a copper cold finger in a helium cryostat.

Lasing at 3.437 THz ($\lambda=87.2$ μm) was obtained in this device at a threshold current density of 840 A/cm^2 at 5 K. Current pulses of 100-ns duration were applied with a pulse repetition frequency of 2 kHz to minimize device heating. Typical emission spectra above threshold are shown in Fig. 2. The emission frequency corresponds to an energy of 14.2 meV, close to the calculated value of 13.9 meV. For much of

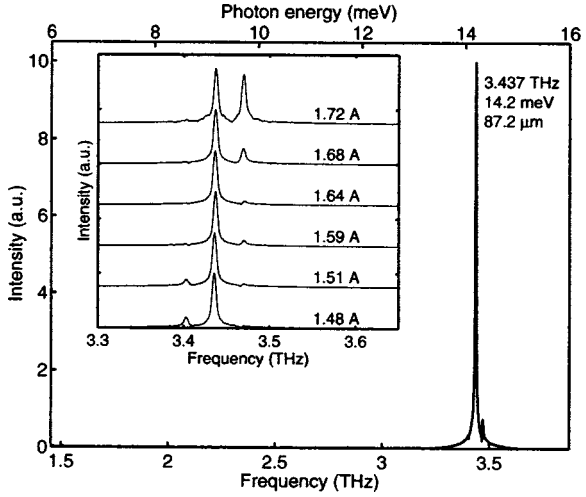

FIG. 2. Emission spectrum above threshold biased at 1.64 A with 100-ns pulses repeated at 10 kHz, at $T=5$ K. Spectra were measured with a Ge:Ga photodetector from Infrared Labs. The inset shows an expanded view of spectra at various bias points, offset for clarity. The spectra were collected using a Nicolet 850 Fourier transform spectrometer in linear-scan mode, and the measured linewidth is limited by the instrumental resolution of 3.75 GHz.

the bias range, the emission is dominated by a single mode, although the spectrum shifts toward higher energy modes with increasing bias (inset, Fig. 2). This is due to the Stark shift of the intersubband gain curve versus applied voltage, which is expected in structures based on a nonintrawell transition.

Measured optical power versus current (P–I) curves at low duty cycle are plotted in Fig. 3(a). Lasing is observed up to 64 K with a power level of 25 μW, compared to the 2.5

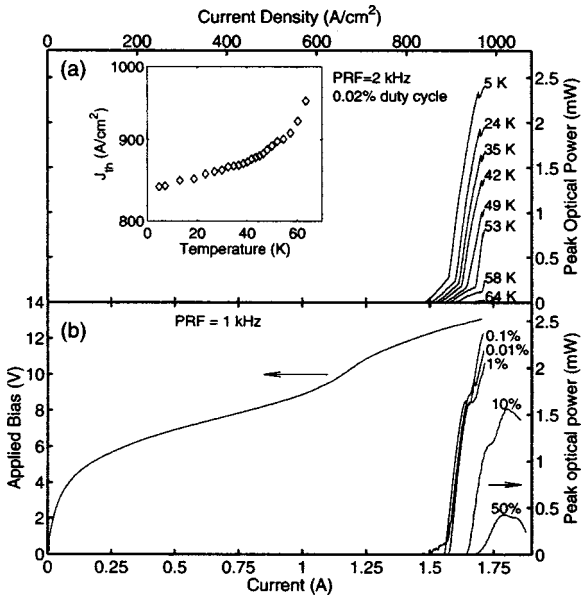

FIG. 3. (a) Emitted light versus current at various temperatures, measured using 100-ns pulses repeated at 2 kHz with a Ge:Ga photodetector. The inset is a semi-log plot of the threshold current density J_{th} versus temperature. (b) Applied bias and peak optical power versus current, collected at various duty cycles with a pulse repetition frequency of 1 kHz. The data was taken with heat sink temperatures of 5 K, except at 10% and 50% duty cycle, which had $T=8$ K and 15 K, due to the large power dissipation. The radiation was measured using a pyroelectric detector (model P4-42, Molectron Inc., Portland, OR) and the measured power level was obtained using the manufacturer's quoted responsivity.

mW observed at 5 K. The inset shows the increase in threshold current density (J_{th}) with temperature. This is caused by the reduction of the upper-state lifetime due to thermally activated LO-phonon scattering, rather than thermal backfilling of the lower state, as in the case of superlattice terahertz lasers.[4] The LO-phonon-based depopulation mechanism is temperature insensitive, and thermal backfilling is expected to be minimal due to the large energy separation between $n=4$ and the collector states 2 and 1, where most electrons reside. Often, a phenomenological function $J_{\text{th}} \sim \exp(T/T_0)$ is used to characterize the temperature dependence in terms of a figure of merit T_0. While our data is poorly fit by any such function, the worst case fit for the two highest temperature points yields $T_0 = 120$ K, which indicates fairly robust temperature performance.

Figure 3(b) displays the voltage versus current, as well as several $P-I$ curves taken for pulses of increasing width repeated at 1 kHz. The peak power remains largely the same for duty cycles below 1%, but for longer pulses, the power drops due to heating. Although 0.5 mW was observed at 50% duty cycle, the device burned out in continuous wave mode, when the silicon nitride layer on the coated facet failed due to thermal stress at the large dc power dissipation level ($\sim$20 W).

The lasing threshold is reached when the modal gain Γg becomes equal to the sum of the waveguide losses α_w and the mirror losses α_m. Based on the Drude conductivity model ($\tau = 0.5$ ps in the active region and 0.1 ps in the contact layers), α_w is calculated to be 7.1 cm^{-1}, with a confinement factor of $\Gamma = 0.29$. For this rear-facet-coated structure, $\alpha_m = 4.9$ cm^{-1}, which requires a threshold bulk gain $g = 40.9$ cm^{-1}. The bulk gain for an intersubband transition is given by

$$g = \frac{\Delta N e^2 f}{2\pi L_p c n \epsilon_0 m^* \Delta \nu}, \tag{1}$$

where L_p is the length of one period, n is the refractive index, m^* is the bulk effective mass of GaAs, and $\Delta\nu$ is the spontaneous emission linewidth in hertz. By using the measured value of $\Delta\nu = 4$ meV (0.97 THz), and the calculated oscillator strength $f_{54} = 0.96$ ($z_{54} = 6.4$ nm), we find this requires a population inversion of $\Delta N = 3.2 \times 10^9$ cm^{-2}, which is approximately 10% of the total sheet density. Earlier tests on a 0.95-mm-long uncoated ridge structure ($\alpha_m = 12.0$ cm^{-1}) failed to produce lasing, so we may assume that the necessary bulk gain $g = 65.3$ cm^{-1} was unattainable. This is close to the $\sim$60 cm^{-1} peak gain value calculated in our preliminary Monte-Carlo simulations.

The maximum measured slope efficiency is approximately 24 mW/A, which is substantially smaller than the ideal value of 1.5 W/A for unity internal quantum efficiency η_i. The expression for slope efficiency is

$$\frac{dP}{dI} = \frac{\hbar\omega}{e} N_p \frac{\alpha_m}{\alpha_m + \alpha_w} \eta_i, \tag{2}$$

where N_p is the number of cascade periods. Aside from imperfect optical collection efficiency, the discrepancy arises since η_i in our structure is certainly less than unity. For example, the feature at $\sim$10 V in the $V-I$ curve seen in Fig. 3(b) corresponds to the injection of current from $n = 1'$ into $n = 4$. The proximity of this feature to the threshold bias of 12 V indicates that some current is likely still being injected into the lower state, reducing efficiency and population inversion. The existence of two slopes in the low duty cycle $P-I$ curves (Fig. 3) supports this understanding. The region of lower slope efficiency is likely due to the alignment of the upper injector state $n = 2'$ with $n = 5$, while most of the electrons remain in $n = 1'$, allowing them to be parasitically injected into $n = 4$. At higher biases, $n = 1'$ is aligned with $n = 5$, which results in a higher slope efficiency. The double-slope feature disappears for longer pulse widths, since lasing in this region occurs only at the beginning of the pulse, before the active region temperature rises significantly.

The performance of this device is quite promising, and hopefully such minor improvements as fabrication of narrower ridges and improved heat sinking will lead to continuous wave operation and pulsed operation at 77 K. Further refinement of the injector should improve efficiency and reduce the threshold current density. We believe that selective LO-phonon-assisted depopulation is a robust scheme that will enable operation at even higher temperatures and still longer wavelengths.

This work is supported by AFOSR, NASA, and NSF. Sandia is a multiprogram laboratory operated by Sandia Corporation, a Lockheed Martin Company, for the U.S. Department of Energy under Contract No. DE-AC04-94AL85000.

[1] M. Helm, P. England, E. Colas, F. DeRosa, and J. S. J. Allen, Phys. Rev. Lett. **63**, 74 (1989).
[2] J. Faist, F. Capasso, D. L. Sivco, C. Sirtori, A. L. Hutchinson, and A. Y. Cho, Science **264**, 553 (1994).
[3] R. Köhler, A. Tredicucci, F. Beltram, H. E. Beere, E. H. Linfield, A. G. Davies, D. A. Ritchie, R. C. Iotti, and F. Rossi, Nature (London) **417**, 156 (2002).
[4] M. Rochat, L. Ajili, H. Willenberg, J. Faist, H. Beere, G. Davies, E. Linfield, and D. Ritchie, Appl. Phys. Lett. **81**, 1381 (2002).
[5] B. Xu, Q. Hu, and M. R. Melloch, Appl. Phys. Lett. **71**, 440 (1997).
[6] B. S. Williams, B. Xu, Q. Hu, and M. R. Melloch, Appl. Phys. Lett. **75**, 2927 (1999).
[7] M. A. Stroscio, M. Kisin, G. Belenky, and S. Luryi, Appl. Phys. Lett. **75**, 3258 (1999).
[8] H. Callebaut, M. S. thesis, Massachusetts Institute of Technology, 2001 (unpublished).
[9] B. S. Williams and Q. Hu, J. Appl. Phys. **90**, 5504 (2001).
[10] B. S. Williams, H. Callebaut, Q. Hu, and J. L. Reno, Appl. Phys. Lett. **79**, 4444 (2001).
[11] J. H. Smet, C. G. Fonstad, and Q. Hu, J. Appl. Phys. **79**, 9305 (1996).
[12] J. Ulrich, R. Zobl, N. Finger, K. Unterrainer, G. Strasser, and E. Gornik, Physica B **272**, 216 (1999).